Available online at www.sciencedirect.com
ScienceDirect
Journal of Sound and Vibration 311 (2008) 1305–1324
JOURNAL OF SOUND AND VIBRATION
www.elsevier.com/locate/jsvi

A novel piezoelectrically actuated flexural/torsional vibrating beam gyroscope

Vikrant Bhadbhade, Nader Jalili*, S. Nima Mahmoodi

Smart Structures and NEMS Laboratory, Department of Mechanical Engineering, Clemson University, Clemson, SC 29634-0921, USA

Received 6 September 2006; received in revised form 17 August 2007; accepted 10 October 2007
Available online 26 November 2007

Abstract

Vibrating beam gyroscopes are fast becoming the most widely used gyroscopes in many commercial applications. This paper deals with a vibrating beam gyroscope consisting of a cantilever beam with rigid mass attached to its end and undergoing coupled flexural–torsional vibrations. The gyroscope can be used to measure the angular velocity of the rotating base of the beam. The primary (flexural) vibrations are produced in the beam using a piezoelectric patch (bender type) actuator. Due to the base rotation, a gyroscopic effect is generated which induces secondary (torsional) vibrations in the beam. First, a detailed mathematical modeling of the system is developed using extended Hamilton's Principle. The system governing equations are solved and simulated using assumed mode model expansion to analyze the gyroscopic coupling produced due to the base rotations. Finally, the effects of secondary base rotation (cross-axis effects) on the performance of the gyroscope are presented. Also, it is shown that the gyroscopic effect increases with increase in base rotation rate, primary excitation amplitude and length of the beam. It is further proven that the secondary base rotations (cross-axis effects) have an adverse effect on the gyroscope performance. Such detailed analysis on the effects of secondary rotation can be utilized to devise elimination strategies in order to improve gyroscopic performance.

1. Introduction

Gyroscope is the most commonly used device for measuring angle of rotation or rate of angular rotation in many applications ranging from automobile stability control to inertial navigation. Based on the operating principle, gyroscopes can be divided into three different categories: (i) spinning mass gyroscopes; (ii) optical gyroscopes; and (iii) vibrating mass gyroscopes. Vibrating mass gyroscopes are the most commonly used existing gyroscopes. They consist of a vibrating mass, which is driven in a primary direction, and attached to a rotating base. In presence of the angular motion of the base, a secondary vibration is induced in the vibrating mass due to the Coriolis effect. By measuring this secondary vibration, the rate of rotation can be determined [1].

Various vibrating elements such as tuning forks, shells, rings and beams are used in vibrating mass gyroscopes [2]. A vibrating beam gyroscope consists of a cantilever beam attached to a moving base as shown

*Corresponding author. Tel.: +1 864 656 5642.
E-mail address: jalili@clemson.edu (N. Jalili).

0022-460X/$ - see front matter © 2007 Elsevier Ltd. All rights reserved.
doi:10.1016/j.jsv.2007.10.017

Nomenclature

$\mathbf{a}_X, \mathbf{a}_Y, \mathbf{a}_Z$	base vectors in X-, Y- and Z-axes, respectively
$\mathbf{a}_x, \mathbf{a}_y, \mathbf{a}_z$	base vectors in x-, y-and z-axes, respectively
b, b_M	width of the beam and end mass, respectively
C_B, C_T	viscous damping coefficient in bending and torsion, respectively
d_{31}	piezoelectric constant of the piezoelectric actuator
E	Young's modulus of elasticity
EI_b, EI_p	flexural rigidity of the beam and piezoelectric actuator, respectively, about Y-axis
f_b	band width
G	shear modulus of elasticity
GJ_b, GJ_p	torsional rigidity of the beam and piezoelectric actuator, respectively
h_M	Height of the end mass
$H(x)$	heaviside function
I_{xb}, I_{yb}, I_{zb}	mass moments of inertia of the beam cross-section about X-, Y-and Z-axes, respectively
I_{xp}	mass moments of inertia of the piezoelectric layer about X-axis
I_{xM}, I_{yM}, I_{zM}	mass moments of inertia of the end mass about X-, Y- and Z-axes, respectively
l_1, l_2	distance of start and end of piezoelectric layer to clamped end of the beam
L, l_M	length of the beam and the end mass, respectively
M	end mass magnitude
$M_p(x,t)$	piezoelectric actuator moment
$p_j(t), q_j(t)$	generalized coordinates
$\mathbf{R}$	transformation matrix
$\mathbf{r}$	position vector
t	time
t_b, t_p	thickness of the beam and actuator, respectively
T	kinetic energy
$u(x,t)$	axial deflection of the beam
$v(x,t)$	lateral deflection of the beam
V	potential energy
$V_p(t)$	voltage applied to piezoelectric actuator
$w(x,t)$	bending deflection of the beam
W_{nc}	non-conservative work
$\phi_j(x)$	jth mode shape in bending
$\theta(x,t)$	torsional deflection of the beam
ζ_{1j}	jth flexural damping ratio of the beam
ζ_{2j}	jth torsional damping ratio of the beam
ρ_b, ρ_p	volumetric densities of the beam and actuator, respectively
$\boldsymbol{\omega}$	angular velocity vector of a beam element about x, y and z axes, $\boldsymbol{\omega} = \{\omega_x, \omega_y, \omega_z\}^{\mathrm{T}}$
ω_{1j}	jth flexural natural frequency of the beam
ω_{2j}	jth torsional natural frequency of the beam
$\boldsymbol{\Omega}$	base rotational frequency vector, $\boldsymbol{\Omega} = \{\Omega_1, \Omega_2 = 0, \Omega_3\}^{\mathrm{T}}$
Ω_1	secondary rotation
Ω_3	primary rotation
$\Omega_{\min}$	resolution frequency
$\psi(x,t)$	bending slope of the beam $(= \partial w(x,t)/\partial x)$
$\Psi_j(x)$	jth mode shape in torsion

in Fig. 1. A flexural vibration is induced in the beam using piezoelectric actuators placed on the beam (drive mode). In presence of the base rotation about the longitudinal axis, the Coriolis force causes secondary flexural vibrations (sense mode) in the beam normal to the drive mode vibrations. By measuring these secondary vibrations using the sensors placed on the beam, the rate of rotation can be consequently determined [3].

In this paper, a second type of vibratory beam gyroscope is considered in which a cantilever beam with a rigid mass attached to its end is subjected to a combination of flexural–torsional vibrations. The operating principle of this gyroscope is very similar to the flexural–flexural vibrating beam gyroscope. A flexural vibration (drive mode) is induced in the beam using piezoelectric actuators placed on the surface of the beam, as shown in Fig. 2. In the presence of the angular rotation of the base about Z-axis, secondary torsional vibrations (sense mode) are induced in the beam due to the Coriolis force. The secondary vibrations are proportional to the rate of rotation of the beam. The rate of rotation can be determined by measuring these secondary vibrations. The effect of the end mass (not shown in Fig. 2) is to improve the performance of the gyroscope by increasing the gyroscopic effect.

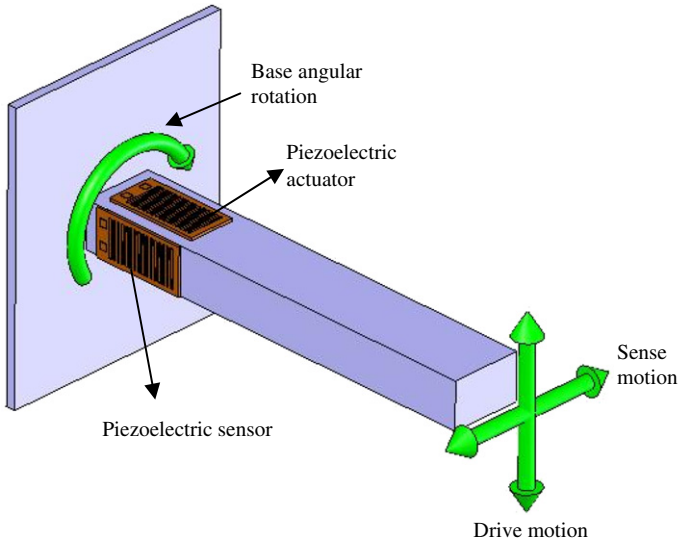

Fig. 1. Schematic of a flexural–flexural vibrating beam gyroscope.

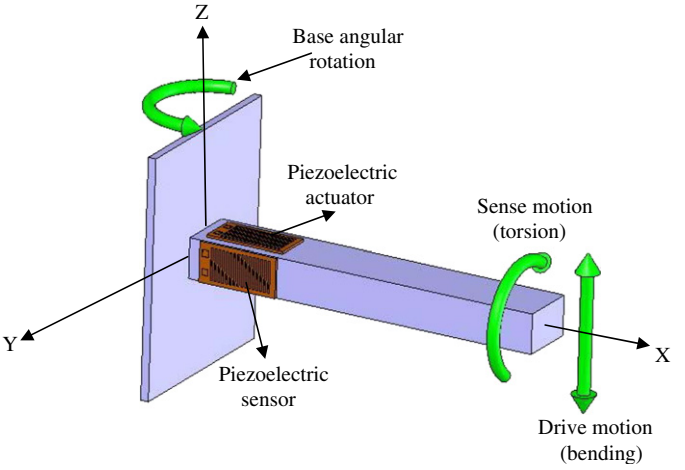

Fig. 2. Schematic of flexural–torsional beam gyroscope.

If the base rotates around the Z-axis only, the measurement of the angular rate will be accurate. In practice, however, the base of the gyroscope is subjected to some secondary rotations as well (e.g. rotation about the longitudinal axis), which can produce significant errors, called as 'cross-axis' effects, in the measurement of the primary angular velocity. These secondary vibrations are one of the major sources of error in the vibrating beam gyroscopes [3].

Due to its practical importance in various applications, many researchers have worked on the problem of coupled bending-torsion vibrations of cantilever beams. Timoshenko and Young [4] developed the theory of coupled flexural–torsional vibrations of thin walled beams and obtained the exact modal solutions. Dokumaci [5] obtained the coupled free vibration frequencies of a cantilever beam. Bercin and Tanaka [6] also studied the coupled flexural–torsional vibrations of beams including warping, shear deformation and rotary inertia effects. Banerjee [7] developed a dynamic stiffness matrix analysis method to obtain the natural frequencies and mode shapes of the coupled Euler–Bernoulli beam. Almost all of these works did not consider the effect of tip mass. Goel [8] and Laura et al. [9] modeled the tip load as point mass using the Euler–Bernoulli beam theory. Bhat and Wagner [10] performed a detailed analysis to develop the frequency equations of a cantilever

beam with tip mass. A more recent attempt to examine the free vibration of a flexible beam with rigid payloads at the tip was made by Kirk and Wiedemann [11]. They used the Euler–Bernoulli theory, but the effect of torsion was not considered. Oguamanam [12] investigated a cantilever beam with a rigid tip mass, whose center of gravity was not coincident with the attachment point. Gokdag and Kopmaz [13] extended the work of Oguamanam by analyzing the coupled flexural–torsional free and forced vibrations of a beam with tip and in span attachments. Most of these works involve the analysis of the cantilever beam when the base is stationary. Recently, Esmaeili, Durali and Jalili in a series of publications [14–16] have studied the flexural–flexural vibrating beam gyroscope with tip mass and subjected to general support motion.

In this paper, detailed equations of motion and boundary conditions governing the coupled flexural–torsional vibrations of a cantilever beam with rigid mass attached to its free end and subjected to general base rotations are derived. The gyroscopic effect produced in the beam due to the base rotation is investigated. These gyroscopic terms in fact produce the coupling between flexural and torsional modes. Previous papers have analyzed the flexural–torsional coupling in a cantilever beam produced due to the asymmetric nature of the end mass or offset between centroid and shear center of the beam cross-section. Moreover, the beam excitation is done using a piezoelectric patch which makes the equations more complex. This configuration has not been dealt with before. Furthermore, the effects of undesirable secondary rotations on the system response are analyzed. By studying the effects of secondary rotations, proper elimination strategies can be devised to improve gyroscope performance.

2. Mathematical modeling

In this section, two linear partial differential equations governing the flexural–torsional motion of the beam are developed. The extended Hamilton's Principle is used to derive the equations of motion. The beam is assumed to follow the Euler–Bernoulli theory and accordingly the effects of warping and shear deformation are neglected. The beam is considered to be a slender type (with small thickness to length ratio).

A schematic of the beam with rigid mass attached is shown in Fig. 3. The beam is considered to be a uniform and straight metallic cantilever beam with length L and mass per unit length $\rho(x)$. A rigid tip mass M of finite dimensions (l_M, b_M, h_M) is attached at the right end of the beam. Inertial coordinate system is denoted by (A_1, A_2, A_3). The moving (rotating) coordinate system is denoted by (X, Y, Z) with orthogonal unit vectors $(\mathbf{a}_X\ \mathbf{a}_Y\ \mathbf{a}_Z)$. Primary bending vibrations $w(x,t)$ are produced in the beam by a piezoelectric actuator attached on the beam surface. The base is subjected to two angular rotations: (i) the primary rotation Ω_3—which is to be measured by the gyroscope and (ii) the secondary rotation Ω_1—which causes errors in the measurement of primary rotation. Due to the primary rotation Ω_3 (about the Z-axis), secondary torsional vibrations $\theta(x,t)$ are induced in the beam.

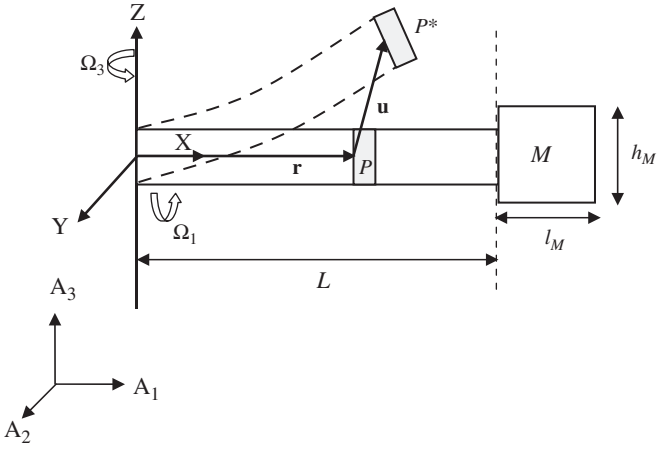

Fig. 3. Cantilever beam kinematics.

2.1. Beam kinematics (translational motion)

As a result of base motion, each point on the neutral axis undergoes an elastic deformation and a rotation. To describe the translational motion of the beam a Cartesian vector $\mathbf{u} = \{u\ v\ w\}^{\mathrm{T}}$ (with three variables defined as: $u_1 = u$ is axial $u_2 = v$ is lateral and $u_3 = w$ is bending deformation) measured in moving coordinate system (X, Y, Z) are used. Point P on the neutral axis of beam is moved to point P^*. The position and velocity of point P^* in reference frame $\{A_i\}$ can be expressed as [14]

$$\mathbf{r}_{p*} = \mathbf{r}_p + \mathbf{u}_{p*}, \tag{1}$$

$$\frac{\mathrm{d}(\mathbf{r}_{p*})}{\mathrm{d}t} = \frac{\mathrm{d}(\mathbf{u}_{p*})}{\mathrm{d}t} + \mathbf{\Omega} \times (\mathbf{r}_p + \mathbf{u}_{p*}), \quad \mathbf{r}_p = s\mathbf{a}_X, \quad \mathbf{u}_{p*} = u\mathbf{a}_X + v\mathbf{a}_Y + w\mathbf{a}_Z. \tag{2}$$

In Eq. (2), $\mathbf{\Omega} = \{\Omega_1, \Omega_2 = 0, \Omega_3\}^{\mathrm{T}}$ is the rotation vector of the base relative to the reference frame (A_1, A_2, A_3) and s is the position of point P in the moving coordinate system. In this case, the beam has no axial and lateral vibrations, hence $u = 0$ and $v = 0$. By simplifying the vector products used in Eq. (2), the velocities of point P^* can be reduced to

$$\frac{\mathrm{d}(\mathbf{r}_{p*})}{\mathrm{d}t} = f\mathbf{a}_X + g\mathbf{a}_Y + h\mathbf{a}_Z, \tag{3}$$

where

$$f = 0, \quad g = -w\Omega_1 + s\Omega_3, \quad h = \frac{\partial w}{\partial t}. \tag{4}$$

Consequently, the translational kinetic energy of the beam is given as

$$T_1 = \frac{1}{2}\int_0^L \rho_b(f^2 + g^2 + h^2)\,\mathrm{d}x. \tag{5}$$

As the mass is attached at the end of the beam, similar procedure is followed to calculate the translational kinetic energy of the mass. Position and velocity of the center of gravity of the mass are given as

$$\mathbf{r}_M = \mathbf{r}_q + \mathbf{u}_{q*} + \mathbf{r}_m, \tag{6}$$

$$\frac{\mathrm{d}(\mathbf{r}_M)}{\mathrm{d}t} = \frac{\mathrm{d}(\mathbf{u}_{q*})}{\mathrm{d}t} + \frac{\mathrm{d}(\mathbf{r}_m)}{\mathrm{d}t} + \Omega \times (\mathbf{r}_q + \mathbf{u}_{q*} + \mathbf{r}_m), \tag{7}$$

where q is the point of attachment of the end mass to the beam with $\mathbf{r}_q = L\mathbf{a}_X$, q^* is the deformed position of point q, and $\mathbf{r}_m$ is the position vector of center of gravity of the end mass from point q^* in the deformed position given as (see Fig. 4)

$$\mathbf{r}_m = \frac{l_M}{2}\cos\psi_L\mathbf{a}_X + \frac{l_M}{2}\sin\psi_L\mathbf{a}_Z, \tag{8}$$

where $\psi_L = \partial w/\partial x|_{x=L}$.

By further simplifying, the velocity of end mass can be written as

$$\frac{\mathrm{d}(\mathbf{r}_M)}{\mathrm{d}t} = f_M\mathbf{a}_X + g_M\mathbf{a}_Y + h_M\mathbf{a}_Z, \tag{9}$$

where

$$f_M = -\frac{l_M}{2}\sin\psi_L\frac{\partial\psi_L}{\partial t},$$

$$g_M = \Omega_3 L - \Omega_1 w_L + \Omega_3\frac{l_M}{2}\cos\psi_L - \Omega_1\frac{l_M}{2}\sin\psi_L,$$

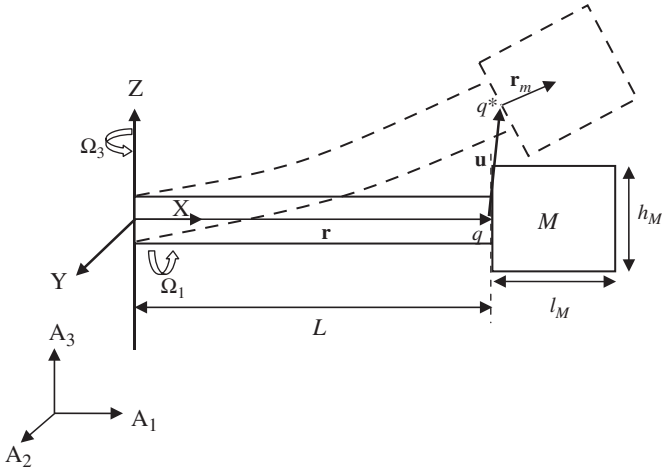

Fig. 4. End mass kinematics.

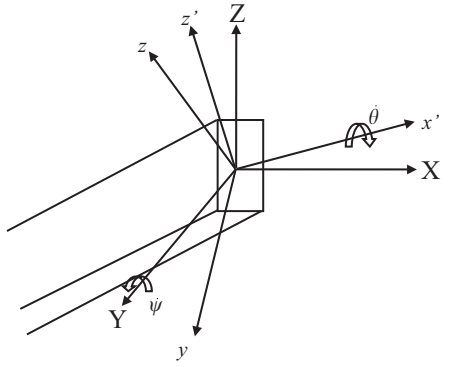

Fig. 5. Euler angle rotations of the beam cross-section.

$$h_M = \frac{\partial w_L}{\partial t} + \frac{l_M}{2}\cos\psi_L \frac{\partial \psi_L}{\partial t}, \tag{10}$$

and $w_L = w(x,t)|_{x=L}$.

Assuming small deflections and ignoring nonlinear terms yields

$$f_M = 0,$$

$$g_M = \Omega_3 L - \Omega_1 w_L + \Omega_3 \frac{l_M}{2} - \Omega_1 \frac{l_M}{2}\psi_L,$$

$$h_M = \frac{\partial w_L}{\partial t} + \frac{l_M}{2}\frac{\partial \psi_L}{\partial t}. \tag{11}$$

Hence, the translational kinetic energy of the end mass is given as

$$T_{1M} = \tfrac{1}{2}M(f_M^2 + g_M^2 + h_M^2). \tag{12}$$

2.2. Beam kinematics (rotational motion)

The deformation of the system from its original configuration is described here using Euler angles (similar to Ref. [17]). As shown in Fig. 5, (X, Y, Z) denote the rotating coordinate system with orthogonal unit vectors

$(\mathbf{a}_X, \mathbf{a}_Y, \mathbf{a}_Z)$. The local curvilinear coordinate system at arclength s in the deformed position is denoted by (x, y, z), with orthogonal unit vectors $(\mathbf{a}_x, \mathbf{a}_y, \mathbf{a}_z)$.

In general, each cross-section of the beam experiences an elastic displacement of its neutral axis and a rotation. The displacement components are already discussed in the previous section. The rotation of the neutral axis, from the undeformed to the deformed position, is described using successive counterclockwise Euler-angle rotations with the angle of rotations denoted, in the order of rotation, by $\psi(x,t)$ and $\theta(x,t)$ as shown in Fig. 5, where $\psi(x,t) = \partial w(x,t)/\partial x$.

The first rotation, ψ about Y-axis, takes (X, Y, Z) coordinate system to $(x', y' = Y, z')$. The second rotation, θ about x'-axis, takes (x', y', z') to the final orientation $(x = x', y, z)$. The three unit vector triads are related to each other in the following manner:

$$\begin{Bmatrix} a_x \\ a_y \\ a_z \end{Bmatrix} = [\mathbf{R}_\theta] \begin{Bmatrix} a_{x'} \\ a_{y'} \\ a_{z'} \end{Bmatrix} = \underbrace{[\mathbf{R}_\theta][\mathbf{R}_\psi]}_{\mathbf{R}} \begin{Bmatrix} a_X \\ a_Y \\ a_Z \end{Bmatrix}, \tag{13}$$

where

$$[\mathbf{R}_\theta] = \begin{bmatrix} 1 & 0 & 0 \\ 0 & \cos\theta & \sin\theta \\ 0 & -\sin\theta & \cos\theta \end{bmatrix}, \quad [\mathbf{R}_\psi] = \begin{bmatrix} \cos\psi & 0 & -\sin\psi \\ 0 & 1 & 0 \\ \sin\psi & 0 & \cos\psi \end{bmatrix}, \tag{14}$$

$$[\mathbf{R}] = \begin{bmatrix} \cos\psi & 0 & -\sin\psi \\ \sin\theta\sin\psi & \cos\theta & \sin\theta\cos\psi \\ \cos\theta\cos\psi & -\sin\theta & \cos\theta\cos\psi \end{bmatrix}. \tag{15}$$

The transformation matrices $[\mathbf{R}_\theta]$, $[\mathbf{R}_\psi]$ and $[\mathbf{R}]$ are orthogonal or unitary matrices, and hence possess the property $[\mathbf{R}]^{-1} = [\mathbf{R}]^{\mathrm{T}}$. On the other hand, the angular velocity of the beam is given as

$$\boldsymbol{\omega} = \Omega_1 \mathbf{a}_X + \Omega_3 \mathbf{a}_Z + \frac{\partial\psi}{\partial t}\mathbf{a}_Y + \frac{\partial\theta}{\partial t}\mathbf{a}_x. \tag{16}$$

The absolute angular velocity $\boldsymbol{\omega}$ of the principle axis system (x, y, z) can be obtained using Eqs. (14)–(16) as follows:

$$\begin{aligned} \boldsymbol{\omega} = {} & \left(\frac{\partial\theta}{\partial t} + \Omega_1\cos\psi - \Omega_3\sin\psi\right)\mathbf{a}_x + \left(\frac{\partial\psi}{\partial t}\cos\theta + \Omega_1\sin\theta\sin\psi + \Omega_3\sin\theta\cos\psi\right)\mathbf{a}_y \\ & + \left(-\frac{\partial\psi}{\partial t}\sin\theta + \Omega_1\cos\theta\sin\psi + \Omega_3\cos\theta\cos\psi\right)\mathbf{a}_z. \end{aligned} \tag{17}$$

Assuming small angles of bending and torsion, the components of the absolute angular velocity of the beam can be given as

$$\begin{aligned} \omega_x &= \left(\frac{\partial\theta}{\partial t} + \Omega_1 - \Omega_3\psi\right), \\ \omega_y &= \left(\frac{\partial\psi}{\partial t} + \Omega_1\theta\psi + \Omega_3\theta\right), \\ \omega_z &= (\Omega_1\psi + \Omega_3). \end{aligned} \tag{18}$$

The rotational kinetic energy of the beam and end mass is therefore given as follows:

$$T_2 = \frac{1}{2}\int_0^L (I_{xb}\omega_x^2 + I_{yb}\omega_y^2 + I_{zb}\omega_z^2)\,\mathrm{d}x, \tag{19}$$

$$T_{2M} = \tfrac{1}{2}(I_{xM}\omega_x^2 + I_{yM}\omega_y^2 + I_{zM}\omega_z^2), \tag{20}$$

where I_{xb}, I_{yb}, I_{zb} and I_{xM}, I_{yM}, I_{zM} are the mass moments of inertia of the beam and end mass, about the X-, Y- and Z-axes, respectively.

2.3. Governing equations of motion

In this section, the extended Hamilton Principle is used to derive the two partial differential equations of motion governing the flexural–torsional vibrations. The extended Hamilton Principle for a dynamic system is stated as

$$\int_{t_1}^{t_2} \{\delta T - \delta V + \delta W_{\mathrm{nc}}\}\,\mathrm{d}t = 0, \tag{21}$$

where T is the total kinetic energy of the system, V is the total potential energy and W_{nc} is the total non-conservative work done on the system. Ignoring the rotary inertia terms, the total kinetic energy of the system is given as

$$T = \frac{1}{2}\int_0^L [\rho(x)(f^2+g^2+h^2) + I_x(x)\omega_x^2]\,\mathrm{d}x + \frac{1}{2}M(f_M^2+g_M^2+h_M^2) + \tfrac{1}{2}(I_{xM}\omega_x^2 + I_{yM}\omega_y^2 + I_{zM}\omega_z^2). \tag{22}$$

The total potential energy of the system can also be written as

$$V = \frac{1}{2}\int_0^L \left[EI_y(x)\left(\frac{\partial^2 w}{\partial x^2}\right)^2 + GJ(x)\left(\frac{\partial\theta}{\partial x}\right)^2\right]\mathrm{d}x, \tag{23}$$

where

$$\rho(x) = (\rho_b + S(x)\rho_p), \quad I_x(x) = (I_{xb} + S(x)I_{xP}),$$

$$EI_y(x) = (EI_b + S(x)EI_P), \quad GJ(x) = (GJ_b + S(x)GJ_P),$$

$$S(x) = H(x-l_1) - H(x-l_2), \tag{24}$$

and EI_b and EI_p are the flexural rigidities of the beam and piezoelectric actuator, respectively, GJ_b and GJ_p are the torsional rigidities of the beam and piezoelectric actuator, respectively, and $H(x)$ is the Heaviside function.

In the Hamiltonian approach, the piezoelectric actuator control moment M_p and the damping effects are collected in the following virtual work expression [18]

$$\delta W_{\mathrm{nc}} = \frac{1}{2}\int_0^L \frac{\partial^2 M_p}{\partial x^2}\,\delta w\,\mathrm{d}x + C_B\int_0^L \frac{\partial w}{\partial t}\delta w\,\mathrm{d}x + C_T\int_0^L \frac{\partial\theta}{\partial t}\delta\theta\,\mathrm{d}x, \tag{25}$$

where

$$M_p = -\tfrac{1}{2}bE_p d_{31}(t_b+t_p)V_p(t)S(x) = M_{p0}V_p(t)S(x). \tag{26}$$

Substituting Eqs. (22)–(26) into Eq. (21), the equations of motion and boundary conditions can be derived as follows (detailed derivation of equations of motion and boundary conditions are given in Appendix A):

$$\rho(x)\left(\frac{\partial^2 w}{\partial t^2} - w\Omega_1^2 + x\Omega_1\Omega_3\right) + C_B\frac{\partial w}{\partial t} - I_x(x)\Omega_3\left(\frac{\partial^2\theta}{\partial t\partial x} + \Omega_3\frac{\partial^2 w}{\partial x^2}\right) + \frac{\partial^2}{\partial x^2}\left(EI_y(x)\left(\frac{\partial^2 w}{\partial x^2}\right)\right) = \frac{\partial^2 M_p}{\partial x^2}, \tag{27}$$

$$I_x(x)\left(\frac{\partial^2\theta}{\partial t^2} + \Omega_3\frac{\partial^2 w}{\partial t\partial x}\right) + C_T\frac{\partial\theta}{\partial t} - \frac{\partial}{\partial x}\left(GJ(x)\left(\frac{\partial\theta}{\partial x}\right)\right) = 0, \tag{28}$$

$$w|_{x=0}=0,\quad \left.\frac{\partial w}{\partial x}\right|_{x=0}=0,\quad \theta|_{x=0}=0, \tag{29}$$

$$I_x(x)\left(\frac{\partial\theta}{\partial t}+\Omega_1-\Omega_3\frac{\partial w}{\partial x}\right)\Big|_{x=L}\Omega_3+M\left(-\Omega_3\left(L+\frac{l_M}{2}\right)+\Omega_1\left(w+\frac{l_M}{2}\frac{\partial w}{\partial x}\right)\right)\Big|_{x=L}\Omega_1$$
$$-M\left(\frac{\partial^2 w}{\partial t^2}+\frac{l_M}{2}\frac{\partial^3 w}{\partial t^2\partial x}\right)\Big|_{x=L}+EI_y(x)\left(\frac{\partial^3 w}{\partial x^3}\right)\Big|_{x=L}=0, \tag{30}$$

$$M\left(-\Omega_1\frac{l_M}{2}-\frac{l_M}{2}\left(\frac{\partial^2 w}{\partial t^2}+\frac{l_M}{2}\frac{\partial^3 w}{\partial t^2\partial x}\right)\Big|_{x=L}\right)+I_{xM}\left(\frac{\partial\theta}{\partial t}+\Omega_1-\Omega_3\frac{\partial w}{\partial x}\right)\Big|_{x=L}\Omega_3$$
$$-I_{yM}\left(\frac{\partial^3 w}{\partial t^2\partial x}+\Omega_1\frac{\partial\theta}{\partial t}+\Omega_3\frac{\partial\theta}{\partial t}\right)\Big|_{x=L}+I_{yM}\left(\frac{\partial^2 w}{\partial t\partial x}+\Omega_1\theta\frac{\partial w}{\partial x}+\Omega_3\theta\right)\Big|_{x=L}\Omega_1\theta_L$$
$$-I_{zM}\left(\Omega_1\frac{\partial w}{\partial x}+\Omega_3\right)\Big|_{x=L}\Omega_1-EI_y(x)\left(\frac{\partial^2 w}{\partial x^2}\right)\Big|_{x=L}=0, \tag{31}$$

$$-I_{xM}\left(\frac{\partial^2\theta}{\partial t^2}-\Omega_3\frac{\partial^2 w}{\partial t\partial x}\right)\Big|_{x=L}+I_{yM}\left(\frac{\partial^2 w}{\partial t\partial x}+\Omega_1\theta\frac{\partial w}{\partial x}+\Omega_3\theta\right)\Big|_{x=L}\Omega_1\frac{\partial w}{\partial x}\Big|_{x=L}$$
$$-I_{yM}\left(\frac{\partial^2 w}{\partial t\partial x}+\Omega_1\theta_L\frac{\partial w}{\partial x}+\Omega_3\theta\right)\Big|_{x=L}\Omega_3-GJ(x)\left(\frac{\partial\theta}{\partial x}\right)\Big|_{x=L}=0, \tag{32}$$

and $\theta_L=\theta(x,t)|_{x=L}$.

In Eqs. (27)–(32), Ω_3 is the primary base rotation velocity that is to be measured using the vibrating beam gyroscope. The secondary base rotation (Ω_1) is considered here to analyze the cross-axis effects produced due to the presence of such secondary rotations. Hence, for simplification, Ω_1 is ignored for further analysis. It will be included in the later sections of the paper. By ignoring Ω_1 in Eqs. (27)–(32), the equations of motion and boundary conditions can be simplified to

$$\rho(x)\frac{\partial^2 w}{\partial t^2}+C_B\frac{\partial w}{\partial t}-I_x(x)\Omega_3\left(\frac{\partial^2\theta}{\partial t\partial x}+\Omega_3\frac{\partial^2 w}{\partial x^2}\right)+\frac{\partial^2}{\partial x^2}\left(EI_y(x)\left(\frac{\partial^2 w}{\partial x^2}\right)\right)=\frac{\partial^2 M_p}{\partial x^2}, \tag{33}$$

$$I_x(x)\left(\frac{\partial^2\theta}{\partial t^2}+\Omega_3\frac{\partial^2 w}{\partial t\partial x}\right)+C_T\frac{\partial\theta}{\partial t}-\frac{\partial}{\partial x}\left(GJ\left(\frac{\partial\theta}{\partial x}\right)\right)=0, \tag{34}$$

$$w|_{x=0}=0,\quad \left.\frac{\partial w}{\partial x}\right|_{x=0}=0,\quad \theta|_{x=0}=0, \tag{35}$$

$$I_x(x)\left(\frac{\partial\theta}{\partial t}-\Omega_3\frac{\partial w}{\partial x}\right)\Big|_{x=L}\Omega_3-M\left(\frac{\partial^2 w}{\partial t^2}+\frac{l_M}{2}\frac{\partial^3 w}{\partial t^2\partial x}\right)\Big|_{x=L}+EI_y(x)\left(\frac{\partial^3 w}{\partial x^3}\right)\Big|_{x=L}=0, \tag{36}$$

$$M\left(-\frac{l_M}{2}\left(\frac{\partial^2 w}{\partial t^2}+\frac{l_M}{2}\frac{\partial^3 w}{\partial t^2\partial x}\right)\Big|_{x=L}\right)+I_{xM}\left(\frac{\partial\theta}{\partial t}-\Omega_3\frac{\partial w}{\partial x}\right)\Big|_{x=L}\Omega_3-I_{yM}\left(\frac{\partial^3 w}{\partial t^2\partial x}+\Omega_3\frac{\partial\theta}{\partial t}\right)\Big|_{x=L}$$
$$-EI_y(x)\left(\frac{\partial^2 w}{\partial x^2}\right)\Big|_{x=L}=0, \tag{37}$$

$$-I_{xM}\left(\frac{\partial^2\theta}{\partial t^2}-\Omega_3\frac{\partial^2 w}{\partial t\partial x}\right)\Big|_{x=L}-I_{yM}\left(\frac{\partial^2 w}{\partial t\partial x}+\Omega_3\theta\right)\Big|_{x=L}\Omega_3-GJ(x)\left(\frac{\partial\theta}{\partial x}\right)\Big|_{x=L}=0. \tag{38}$$

As seen from Eqs. (33) and (34), the system governing equations are coupled through the base rotation velocity Ω_3. The base rotation gives rise to the gyroscopic terms such as $I_x\Omega_3(\partial^2\theta/\partial t\partial x)$ and $I_x\Omega_3(\partial^2 w/\partial t\partial x)$, causing dynamic coupling between the two vibration modes proportional to the rate of rotation. In the absence of the base rotation, the governing equations become decoupled.

3. Frequency equation derivations

In this section, frequency equations are derived similar to Ref. [12]. Assuming harmonic motion with frequency ω, the solutions of the equations of motions can be represented in the following form:

$$w(x,t) = LP(x)e^{i\omega t}, \quad \theta(x,t) = Q(x)e^{i\omega t}, \tag{39}$$

where $P(x)$ and $Q(x)$ are the amplitudes of the sinusoidally varying vertical displacement and torsional rotation, respectively. Furthermore, a set of non-dimensional parameters can be introduced for simplifying the mathematical analysis. These parameters are defined as follows:

$$\kappa = \frac{x}{L}, \quad l_a = \frac{l_M/2}{L}, \quad \lambda^4 = \frac{\rho_b L^4 \omega^2}{EI}, \quad \gamma^2 = \frac{EI_b}{GJ_b},$$

$$\mu^2 = \frac{J}{bt_b L^2}, \quad M_t = \frac{M}{\rho_b L} \quad \text{and} \quad \tau_{ij} = \frac{I_{ij}}{\rho_b L^3} \quad i,j = x,y,z. \tag{40}$$

Notice that the effect of flexural and torsional rigidities variation along the beam length is assumed to be negligible (only for the purpose of deriving the frequency equation), that is, $EI_y(x) = EI_b$ and $GJ(x) = GJ_b$.

Substituting Eqs. (39) and (40) into Eqs. (33)–(38) yields the following set of non-dimensional equations of motion and boundary conditions:

$$P^{IV} + \left(\frac{I_{xb}L^2\Omega_3^2}{EI}\right)P'' - (\lambda^4)P + \left(I_{xb}\Omega_3 iL\lambda^2\sqrt{\frac{1}{\rho_b EI}}\right)Q' = 0, \tag{41}$$

$$Q'' + \left(\frac{I_{xb}\lambda^4\gamma^2}{\rho_b L^4}\right)Q - \left(I_{xb}\Omega_3 i\lambda^2\gamma\sqrt{\frac{1}{GJ\rho_b L^4}}\right)P' = 0, \tag{42}$$

$$P(0) = 0, \quad P'(0) = 0, \quad Q(0) = 0, \tag{43}$$

$$\left(I_{xb}i\Omega_3\lambda^2\sqrt{\frac{1}{\rho_b EI}}\right)Q(1) + \left(\frac{I_{xb}L^2\Omega_3^2}{EI} + \lambda^4 M_t l_a\right)P'(1) + \left(\lambda^4 M_t\right)P(1) + P'''(1) = 0, \tag{44}$$

$$(\lambda^2 i\Omega_3(\sqrt{\tau_{xx}}\alpha_x + \sqrt{\tau_{yy}}\alpha_y))Q(1) + (\lambda^4 M_t l_a^2 + \lambda^4\tau_{yy})P'(1) + (\lambda^4 M_t l_a + \alpha_x^2\Omega_3^2)P(1) - P''(1) = 0, \tag{45}$$

$$\left(\frac{\lambda^4\gamma^2\tau_{xx}}{L} + \beta_y^2\Omega_3^2\right)Q(1) - \left(\lambda^2 i\gamma\Omega_3\left(\sqrt{\frac{\tau_{xx}}{L}}\beta_x + \sqrt{\frac{\tau_{xx}}{L}}\beta_y\right)\right)P'(1) - Q'(1) = 0, \tag{46}$$

where

$$\alpha_x = \sqrt{\frac{LI_{xM}}{EI}}, \quad \alpha_y = \sqrt{\frac{LI_{yM}}{EI}}, \quad \beta_x = \sqrt{\frac{I_{xM}}{EI}}, \quad \beta_y = \sqrt{\frac{I_{yM}}{EI}}, \tag{47}$$

and $i = \sqrt{-1}$. In the above equations, $()'$ represents the derivative with respect to spatial variable x. Based on the boundary conditions identified by Eq. (43), the solution to the governing equations (Eqs. (41)–(42)) can be written as

$$P(\kappa) = A_1(\sin(\lambda\kappa) - \sinh(\lambda\kappa)) + A_2(\cos(\lambda\kappa) - \cosh(\lambda\kappa)), \tag{48}$$

$$Q(\kappa) = B_1\sin(\lambda^2\gamma\kappa). \tag{49}$$

These equations are now substituted into the remaining boundary conditions (Eqs. (44)–(46)) to obtain a set of equations which can be written in the matrix notation as

$$\mathbf{A}_{3\times3}\mathbf{X}_{3\times1} = 0, \tag{50}$$

where $\mathbf{X} = [B_1\ A_1\ A_2]^T$ is the column vector of the coefficients of the general solutions (Eqs. (48) and (49)). The frequency equation can now be obtained by equating the determinant of matrix $\mathbf{A}$ to zero. Along with the

various geometric parameters such as beam dimensions, tip mass dimensions and magnitude of the tip mass, the determinant of the matrix **A** is also a function of base rotation velocity Ω_3 and the non-dimensional natural frequency λ. The frequency equation may be written as

$$\det(\mathbf{A}) = f\ (\text{Geometry}, \Omega_3, \lambda) = 0. \tag{51}$$

The frequency equation given by Eq. (51) is too lengthy to be given here. It can be shown that it reduces to that of a clamped-free beam undergoing planar bending vibrations by putting $\Omega_3 = 0$, $M_t = 0$ and $\tau_{xx} = \tau_{yy} = 0$, or that of a clamped-tip mass beam by letting $\Omega_3 = 0$ and $\tau_{xx} = \tau_{yy} = 0$.

To analyze the effect of base rotation on the non-dimensional natural frequencies of the systems, various values of base rotation rate within the interval of 0–70 rad/s are considered. Fig. 6 shows the variation of the first two natural frequencies as the rate of angular rotation is varied. The physical properties of the beam and the tip mass used for these simulations are given in Table 1. It can be seen that the natural frequencies of the system increase, although slightly, as the base rotation rate increases. This was expected as the base rotation induces geometrical stiffening in beams and results in increasing all the frequencies. However, for the base rotation rates considered in this paper (0–70 rad/s) and the physical parameters taken here (Table 1), the first two natural frequencies did not change significantly. For all practical purposes and for the subsequent simulations and analysis, the fundamental frequencies of a cantilever beam undergoing bending and torsion

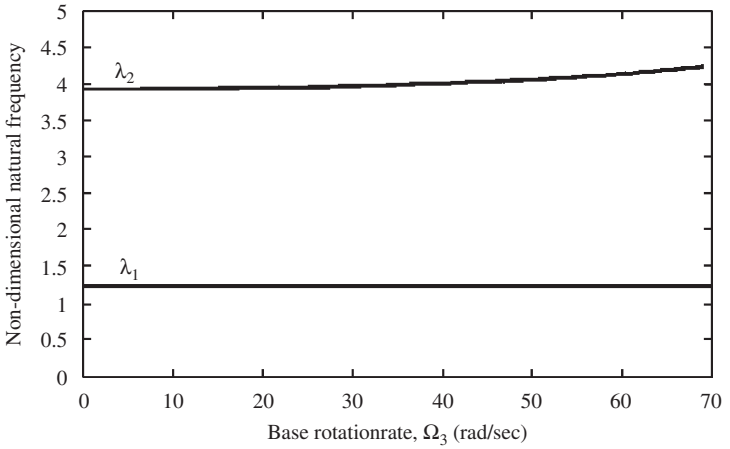

Fig. 6. Variation of beam non-dimensional natural frequency (λ) with base rotation rate (Ω_3).

Table 1
Physical parameters of the system

Properties	Symbol	Value	Unit
Beam length	L	0.15	m
Beam thickness	t_b	0.8×10^{-3}	m
Beam width	b	1.5×10^{-2}	m
Beam density	ρ_b	3960	kg/m^3
Beam elastic modulus	E	70	GPa
Beam shear modulus	G	30	GPa
End mass width	b_M	0.02	m
End mass height	h_M	0.02	m
End mass length	l_M	0.02	m
First flexural damping ratio	ζ_{11}	1	%
Second flexural damping ratio	ζ_{12}	0.16	%
First torsional damping ratio	ζ_{21}	1	%
Second torsional damping ratio	ζ_{22}	0.33	%

with a rigid mass attached to its end, but without the base rotation, can be safely used for the case in which the base of the beam is rotating.

4. Numerical simulations and results

For numerical simulations, the assumed mode model (AMM) expansion is used to truncate the original partial differential governing equations of motion to that of ordinary differential equations [3,18,19]. Using the AMM method, the lateral displacement w and torsional displacement θ are assumed as linear functions of assumed modes and generalized coordinates as

$$w(x,t) = \sum_{j=1}^{n} \phi_j(x) p_j(t),$$

$$\theta(x,t) = \sum_{j=1}^{n} \psi_j(x) q_j(t), \tag{52}$$

where $\phi_j(x)$ and $\psi_j(x)$ are the mode shapes of a cantilever beam (with no base rotation and rigid mass) under bending and torsion, respectively; and $p_j(t)$ and $q_j(t)$ are the generalized coordinates for bending and torsion, respectively. The mode shapes used for this case are given as

$$\phi(x) = (\sin\beta_n x - \sinh\beta_n x) - \alpha_n(\cos\beta_n x - \cosh\beta_n x), \tag{53}$$

$$\psi(x) = \sin\left[\frac{(2n+1)\pi x}{2L}\right], \tag{54}$$

where

$$\alpha_n = \left(\frac{\sin\beta_n L - \sinh\beta_n L}{\cos\beta_n L + \cosh\beta_n L}\right) \quad \text{and} \quad \beta_n^4 = \frac{\rho_b \omega_{1n}^2}{EI_b}. \tag{55}$$

Although the cantilever beam is subjected to a base rotation and it has a rigid mass attached to its end, the mode shapes for a regular cantilever beam (with no base rotation and rigid mass) are used. The mode shapes given by Eqs. (53) and (54) satisfy only the geometric boundary conditions for the beam (Eq. (29)) but they do not satisfy the natural boundary conditions (Eqs. (30)–(32)). Hence, these mode shapes are rather admissible functions.

Using these admissible functions does not significantly affect the results due to the following reasons: (i) the base rotation rates considered in this paper (0–70 rad/s) do not considerably change the natural frequencies of the beam. Hence, the mode shapes for the beam without any base rotations can be safely used and (ii) the mode shapes for the cantilever beam with a rigid mass attached to its end are very complicated. Since the main aim is to analyze the gyroscopic effect in the beam, for simplifying the analysis, the end mass can be neglected. This is a valid simplifications since $\phi(x)$ and $\psi(x)$ are admissible functions. Using these admissible functions does not significantly alter the results as the generalized coordinates $p_j(t)$ and $q_j(t)$ in Eq. (52) change accordingly to give correct response for $w(x,t)$ and $\theta(x,t)$.

The governing equations of motion can now be obtained by substituting Eq. (52) into Eqs. (33)–(34) as follows:

$$\begin{aligned} &\mathbf{M}_1\ddot{\mathbf{p}}(t) + \mathbf{C}_B\dot{\mathbf{p}}(t) + \mathbf{C}_1\dot{\mathbf{q}}(t)\Omega_3 + (\mathbf{K}_1 + \mathbf{D}_1\Omega_3^2)\mathbf{p}(t) = \mathbf{F}_1, \\ &\mathbf{M}_2\ddot{\mathbf{q}}(t) + \mathbf{C}_T\dot{\mathbf{q}}(t) + \mathbf{C}_2\dot{\mathbf{p}}(t)\Omega_3 + \mathbf{K}_2\mathbf{q}(t) = 0, \end{aligned} \tag{56}$$

where

$$\begin{aligned} M_{1ij} &= \int_0^L \rho(x)\phi_i(x)\phi_j(x)\,\mathrm{d}x, \quad C_{1ij} = \int_0^L I_x(x)\phi_i(x)\psi_j'(x)\,\mathrm{d}x, \\ K_{1ij} &= \int_0^L EI(x)\phi_i''(x)\phi_j''(x)\,\mathrm{d}x, \quad D_{1ij} = \int_0^L I_x(x)\phi_i(x)\phi_j''(x)\,\mathrm{d}x, \\ F_{1i} &= M_{p0}V_p(t)[\phi_i'(l_2) - \phi_i'(l_1)], \end{aligned}$$

$$M_{2ij} = \int_0^L I_x(x)\psi_i(x)\psi_j(x)\,\mathrm{d}x, \quad C_{2ij} = \int_0^L I_x(x)\psi_i(x)\phi'_j(x)\,\mathrm{d}x,$$

$$K_{2ij} = \int_0^L GJ(x)\psi'_i(x)\psi'_j(x)\,\mathrm{d}x, \quad i,j = 1,2,\ldots,n,$$

$$C_{Bij} = 2\zeta_{1i}\omega_{1j} \quad \text{for } i = j \text{ and } C_{Bij} = 0 \text{ for } i \neq j,$$

$$C_{Tij} = 2\zeta_{2i}\omega_{2j} \quad \text{for } i = j \text{ and } C_{Tij} = 0 \text{ for } i \neq j,$$

$$\mathbf{p} = \{p_1, p_2, \ldots, p_n\}^{\mathrm{T}}, \mathbf{q} = \{q_1, q_2, \ldots, q_n\}^{\mathrm{T}}.$$

Equations of motion, given by Eq. (56), are solved for first two modes using MATLAB and system parameters given in Table 1. The number of modes in AMM expansion was selected based on the beam natural frequencies, range of piezoelectric excitation frequency and base rotational rates.

4.1. System response to base rotations

As explained earlier, the gyroscopic coupling in the system is obtained when the beam is subjected to base rotation. Fig. 7 shows the torsional output (gyroscopic coupling) from the system when it is subjected to base rotation of constant angular velocity. It should be noticed that in order to provide response with higher amplitude, the excitation frequency is chosen close to first flexural natural frequency. Therefore, beating phenomenon is observed in all the results. As seen from Fig. 7(b), the output in the sense direction is zero when the base of the beam is stationary ($\Omega_3 = 0$). This shows that in the absence of base rotation, there is no gyroscopic coupling present in the system. As seen from Figs. 7(d) and (f), the amplitude of the sense direction doubles (0.015−0.3 μrad) as the base rotation velocity increases from 20 to 40 rad/s; but without any increase in the drive direction amplitude. This demonstrates that, as the magnitude of the base rotation increases, due to the corresponding increase in the gyroscopic coupling, secondary (torsional) vibrations also increase proportionally. Hence, it can be concluded that the amplitude of the secondary torsional vibrations is directly proportional to the magnitude of the base rotation and in the absence of base rotation, the gyroscope does not produce any secondary output. This is an important conclusion as it proves the effectiveness of this type of gyroscope as a device for measuring base angular velocity [22].

4.2. System response to input excitations

Fig. 8 shows the variation of system output (gyroscopic effect) with change in the excitation amplitude. The beam is excited with different piezoelectric voltages at constant base rotation velocity ($\Omega_3 = 20$ rad/s). It is clearly seen that the gyroscopic effect is a function of the amplitude of primary excitation. When the primary excitation is zero, gyroscopic effect is not produced and there are no secondary vibrations (as shown in Fig. 8(a–b)). As the excitation amplitude increases, the torsional output of the system increases proportionally.

4.3. System response to varying beam length

The gyroscopic effect produced by this type of gyroscope is also a function of the length of the cantilever beam. If the length of the beam increases, the amplitude of the primary (flexural) vibrations increases. This increase in the primary amplitude produces a corresponding increase in the secondary output (gyroscopic coupling). Fig. 9 shows the variation in the system output (gyroscopic effect) with change in the length of the beam. Length of the beam is varied from 0.15 to 0.25 m while keeping all other parameters (i.e., angular velocity of the base rotation, piezoelectric excitation voltage) constant. As seen from the figure, the drive direction as well as the sense direction amplitudes increase as the length of the beam increases.

4.4. Resolution study

In this section, sensitivity of the presented gyroscope is investigated. Refs. [20,21] are utilized in order to study the sensitivity of the system. Since w represents the primary motion which is produced due to

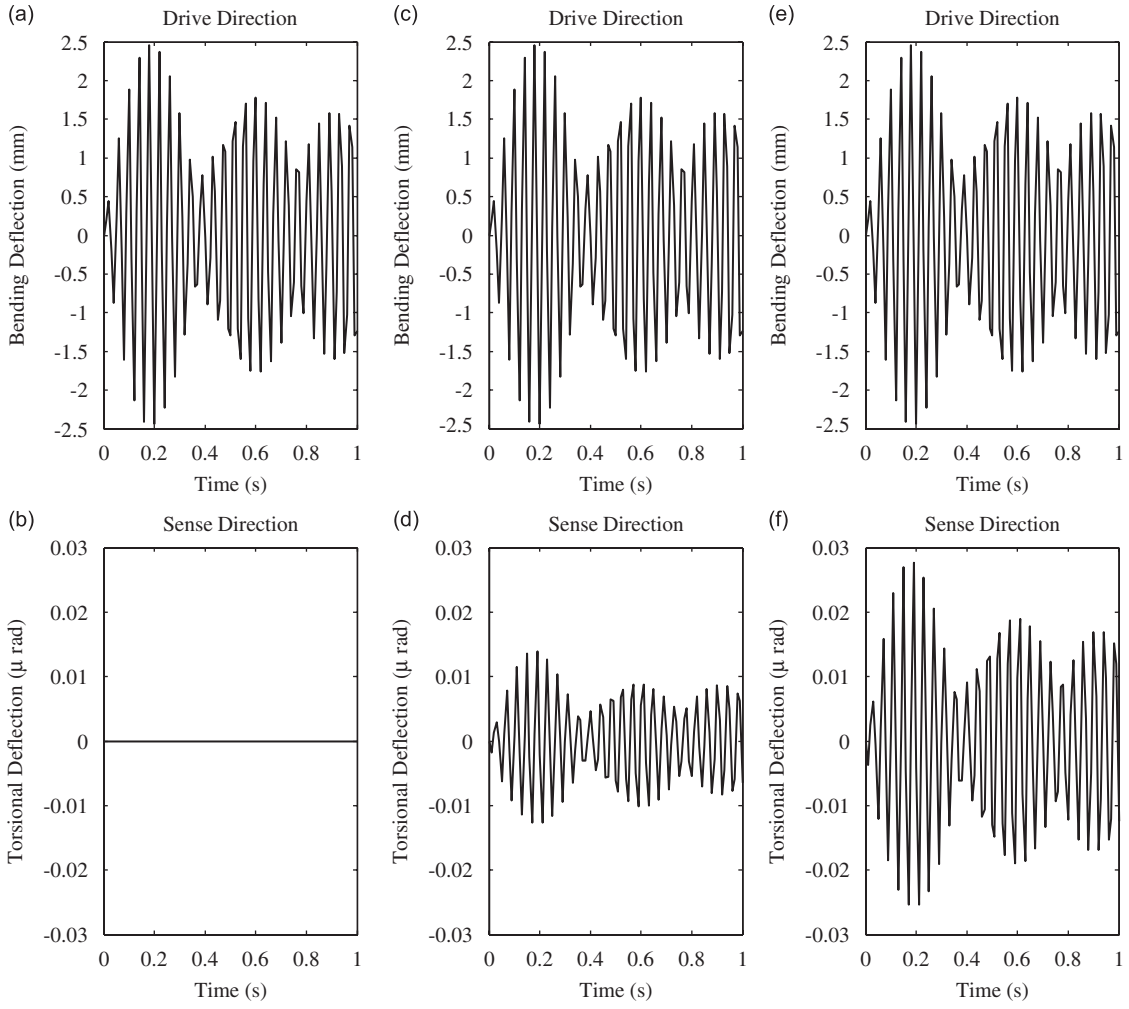

Fig. 7. System response (bending deflection $w(L,t)$ and torsional deflection $\theta(L,t)$) to different base *primary* rotational rates: (a), (b) $\Omega_3 = 0\,\text{rad/s}$, (c), (d), $\Omega_3 = 20\,\text{rad/s}$, and (e), (f) $\Omega_3 = 40\,\text{rad/s}$.

piezoelectric actuation, the secondary motion (θ) is driven due to coupling of flexural and torsional vibrations. Sensitivity is defined as the ratio of variations of secondary (induced gyroscopic) motion with respect to variations of primary rotation. Hence, the expression for sensitivity can be expressed as

$$\text{Sensitivity} = \frac{\partial\theta(L,t)}{\partial\Omega_3}, \tag{58}$$

where $\theta(L,t)$ is the torsional deflection at the free end of the beam. Using Eq. (52), Eq. (58) can be written as

$$\text{Sensitivity} = \sum_{j=1}^{n} \psi_j(L)\frac{\partial q_j^m}{\partial\Omega_3}, \tag{59}$$

where q_j^m is the steady-state amplitude of the jth generalized coordinate $q_j(t)$ (for torsion). Since analytical solution to expression (59) is almost impossible, numerical methods can be utilized to calculate the sensitivity values given by Eq. (59). Consequently, one could approximate (59) with

$$\text{Sensitivity} = \sum_{j=1}^{n} \psi_j(L)\frac{\Delta q_j^m}{\Delta\Omega_3}. \tag{60}$$

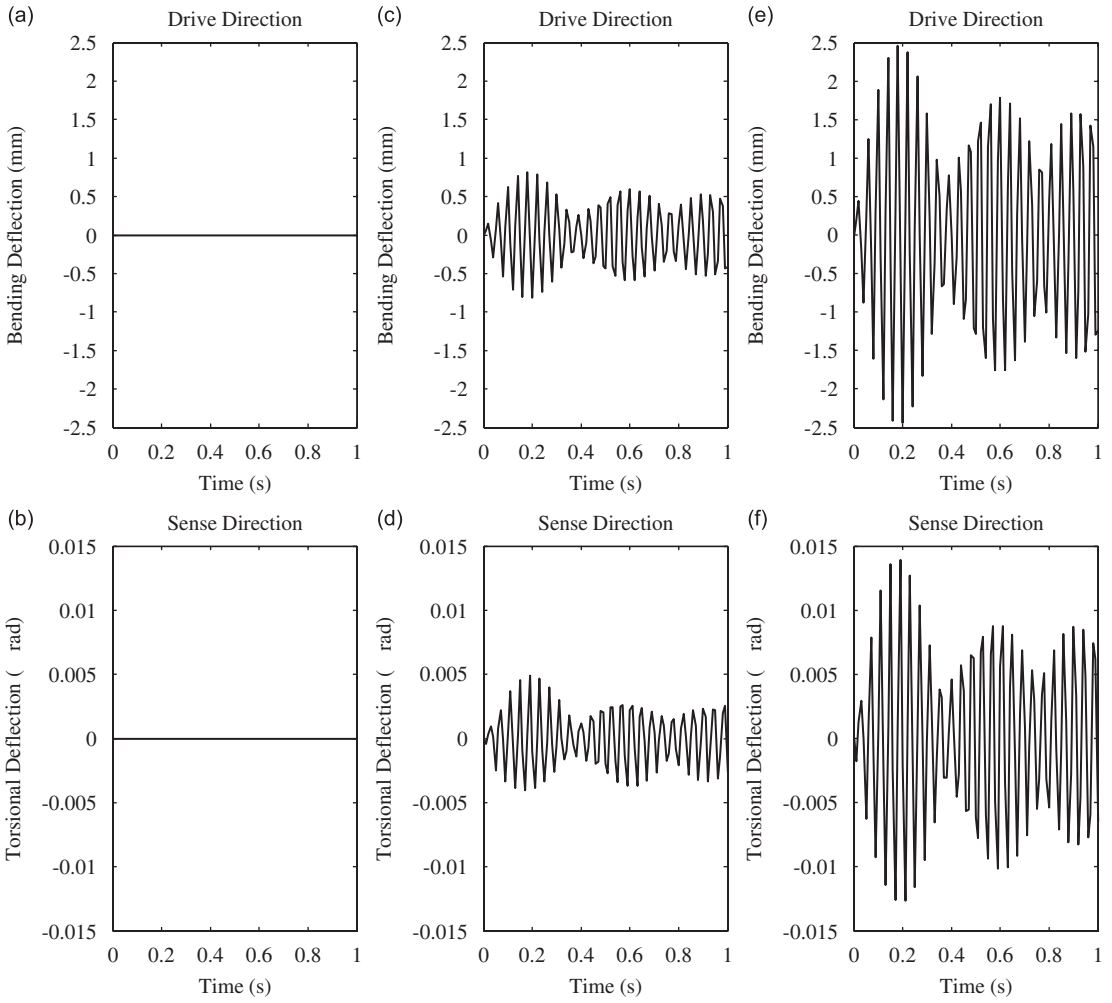

Fig. 8. System response (bending deflection $w(L,t)$ and torsional deflection $\theta(L,t)$) to different piezoelectric excitation amplitude: (a), (b) $V_p = 0\,\mathrm{V}$, (c), (d) $V_p = 100\,\mathrm{V}$, and (e), (f) $V_p = 300\,\mathrm{V}$.

Considering the base rotation range assumed here (0–70 rad/s), the sensitivity expression (60) is numerically calculated at several distinct base rotation rates within this range and when taking the first two modes of vibration in both bending and torsion. The summary of the results is given here; for $\Omega_3 = 20\,\mathrm{rad/s}$, Sensitivity = 6.21 ns and for $\Omega_3 = 40\,\mathrm{rad/s}$, Sensitivity = 11.35 ns. As seen, the sensitivity almost doubles for $\Omega_3 = 40\,\mathrm{rad/s}$ when compared to $\Omega_3 = 20\,\mathrm{rad/s}$. It is interesting to note that these results also match the sensor outputs for these two frequencies given in Fig. 7(d) for $\Omega_3 = 20\,\mathrm{rad/s}$ and Fig. 7(f) for $\Omega_3 = 40\,\mathrm{rad/s}$. That is, the higher the sense direction amplitude, the more sensitive gyroscope becomes.

5. Cross-axis effects

The vibrating beam gyroscope is used to measure the rotational rate around one of the axes. In practice, however, there are always some secondary rotations present in the system. These secondary base rotations can produce significant errors in measurement of the gyroscope output. These errors are referred to as 'cross-axis' effects. In this section, the effects of these secondary vibrations on the output of the gyroscope are discussed.

The base rotation along the longitudinal axes (Ω_1) is considered as the secondary rotations. Equations of motion and boundary conditions for this case have been derived earlier (see Eqs. (27)–(32)).

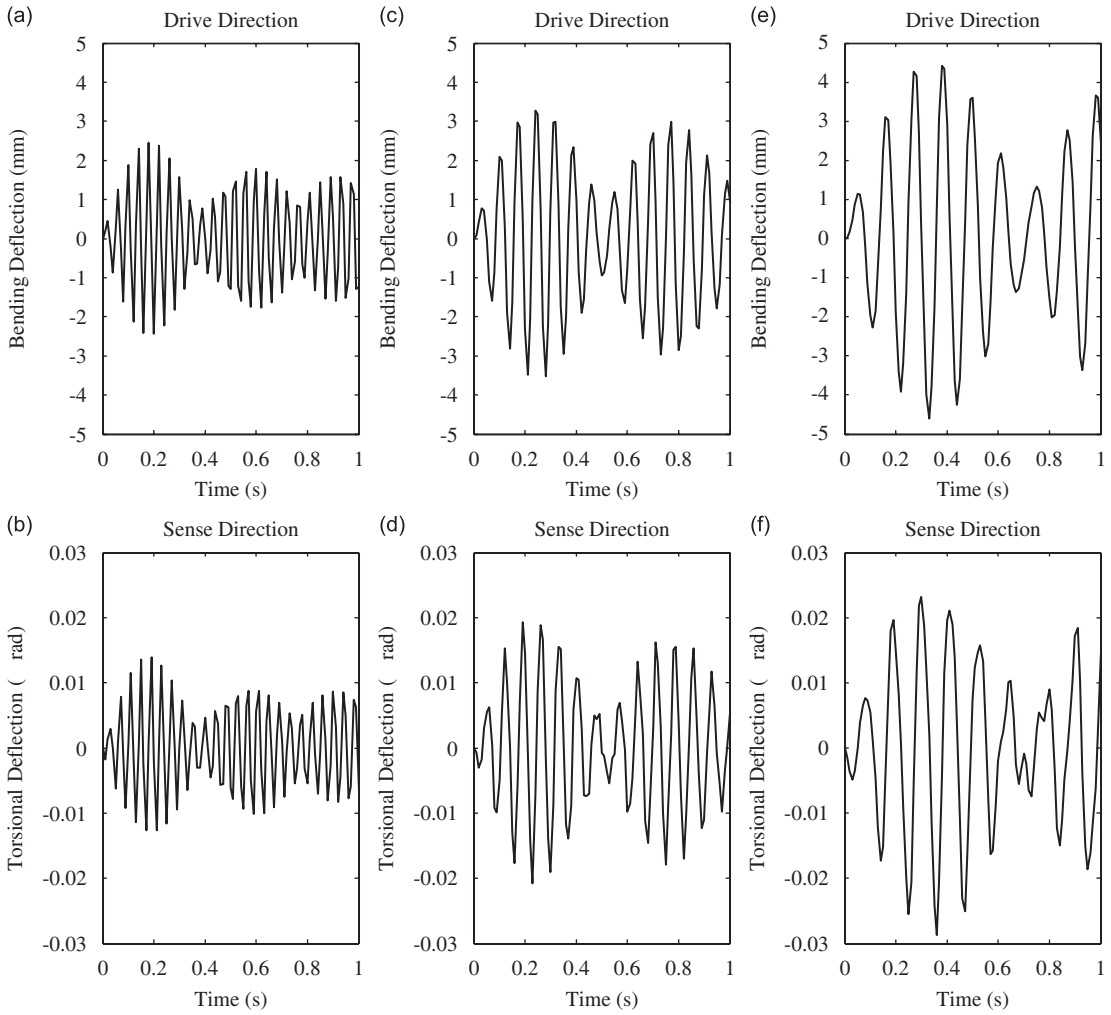

Fig. 9. System response (bending deflection $w(L,t)$ and torsional deflection $\theta(L,t)$) to beam length variation: (a), (b) $L = 0.15$ m, (c), (d) $L = 0.20$ m, and (e), (f) $L = 0.25$ m.

5.1. Simulations using AMM method

Similar to the procedure outlined in Section 4, the AMM method can be used to truncate the original partial differential governing equations of motion to that of ordinary differential equations. The lateral displacement w and torsional displacement θ are assumed as linear functions of assumed modes and generalized coordinates as shown in Eq. (52). The system governing equations can now be obtained by substituting Eq. (52) into Eqs. (27) and (28) as follows:

$$\begin{aligned}&\mathbf{M}_1\ddot{\mathbf{p}}(t) + \mathbf{C}_B\dot{\mathbf{p}}(t) + \mathbf{C}_1\dot{\mathbf{q}}(t)\Omega_3 + (\mathbf{K}_1 + \mathbf{D}_1\Omega_3^2 - \mathbf{M}_1\Omega_1^2)\mathbf{p}(t) + \mathbf{G}_1\Omega_1\Omega_3 = \mathbf{F}_1,\\ &\mathbf{M}_2\ddot{\mathbf{q}}(t) + \mathbf{C}_T\dot{\mathbf{q}}(t) + \mathbf{C}_2\dot{\mathbf{p}}(t)\Omega_3 + \mathbf{K}_2\mathbf{q}(t) = 0,\end{aligned} \tag{61}$$

where

$$G_{1i} = \int_0^L \rho(x)x\phi_i(x)\,\mathrm{d}x, \quad i = 1,2,\ldots,n \tag{62}$$

and the rest of the coefficients have been defined in Eq. (57). Equations of motion given by Eq. (61) are solved for the first two modes using MATLAB.

System response with secondary base rotations: Fig. 10 depicts the output of the gyroscope when subjected to primary (Ω_3) as well as secondary (Ω_1) base rotations of constant values. To analyze the "cross-axis" effects, the magnitude of the secondary base rotation (Ω_1) is varied from 0–0.2 rad/s while keeping a constant piezoelectric excitation voltage ($V_p = 300$ V) and primary base rotation ($\Omega_3 = 20$ rad/s). As seen from Fig. 10(a), the gyroscopic output is not affected when the secondary base rotation is zero. The torsional output produced by the system, depicted in Fig. 10(a), is similar to the one shown in Fig. 7(d). Fig. 10(b–d) shows the gyroscopic output of the system when the base has secondary rotations of very small magnitude (0.05–0.2 rad/s). It can be seen that the gyroscopic output increases significantly even for such a small secondary rotation. This increased output could be interpreted as a gyroscope output due to the primary base rotation and can hence produce errors in the measurement. This is an important factor to take into account in the design of the vibrating beam gyroscope and effective control strategies have to be developed to eliminate the "cross-axis" effects.

6. Conclusions

A detailed mathematical modeling of a vibrating beam gyroscope undergoing flexural–torsional vibrations was presented in this paper. Furthermore, by simulating the system, the presence of the gyroscopic coupling

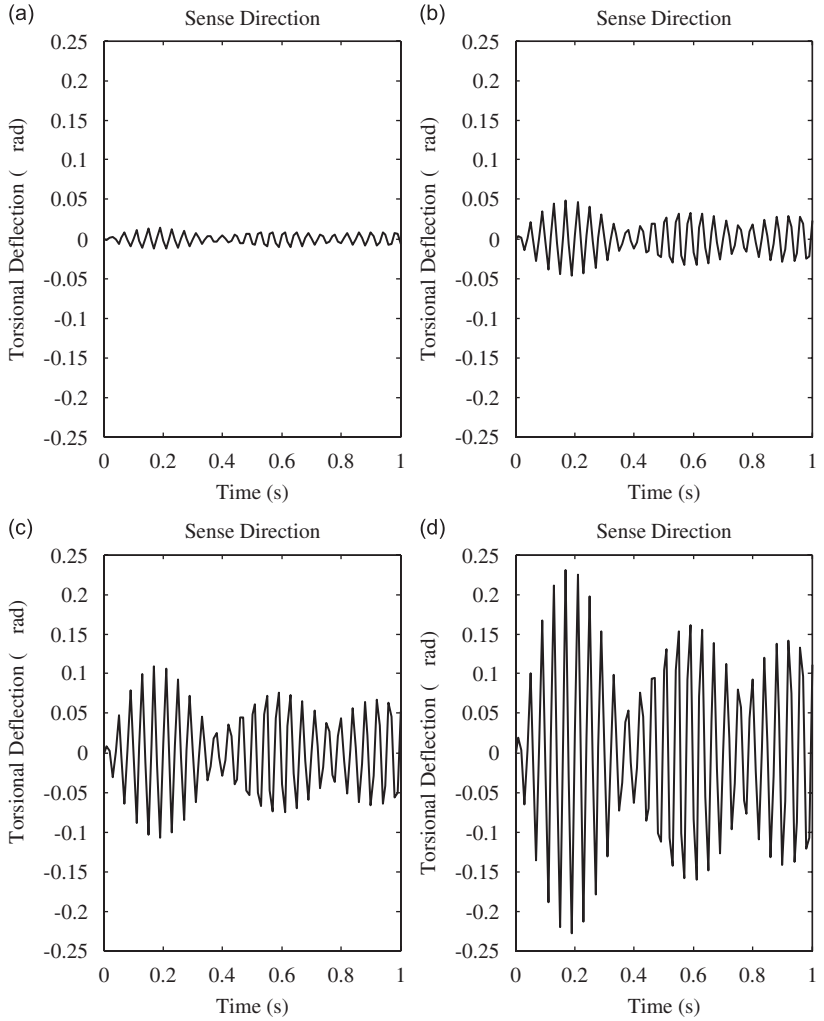

Fig. 10. Cross-axis effect; system response (torsional deflection $\theta(L,t)$) to different *secondary* base rotational rates (with $\Omega_3 = 20$ rad/s): (a) $\Omega_1 = 0$ rad/s, (b) $\Omega_1 = 0.05$ rad/s, (c) $\Omega_1 = 0.1$ rad/s, and (d) $\Omega_1 = 0.2$ rad/s.

present in the system was validated. It was concluded that the magnitude of the gyroscopic coupling increases with increase in the angular velocity as well as primary excitation amplitude. Finally, the effects of secondary base rotations (cross-axis effects) on the gyroscopic output signals were presented. It was inferred that the presence of cross-axis effects can produce significant errors in the gyroscopic output and efficient control strategies have to be developed to reduce these effects.

Appendix A. Derivation of equations of motion

The extended Hamilton's Principle is given as

$$\int_{t_1}^{t_2} \{\delta T - \delta V + \delta W_{\mathrm{nc}}\}\,\mathrm{d}t = 0. \tag{A.1}$$

Using the expressions for kinetic energy, potential energy and virtual work, and ignoring damping, different components of Eq. (A.1) can be expressed as:

Kinetic energy:

$$\begin{aligned}\int_{t_1}^{t_2} \delta T_b\,\mathrm{d}t = \int_{t_1}^{t_2}\int_0^L [&\rho(x)(f\delta f + g\delta g + h\delta h) + I_{xb}(x)\omega_x\delta\omega_x \\ &+ I_{yb}(x)\omega_y\delta\omega_y + I_{zb}(x)\omega_z\delta\omega_z]\,\mathrm{d}x\,\mathrm{d}t.\end{aligned} \tag{A.2}$$

Substituting values of $f, g, h, \omega_x, \omega_y$ and ω_z from Eqs. (3) and (22), Eq. (A.2) can be simplified as follows:

$$\begin{aligned}\int_{t_1}^{t_2} \delta T_b\,\mathrm{d}t = \int_{t_1}^{t_2}\int_0^L \Bigg[&\rho(x)\left(0 + g(-\Omega_1\delta w) + h\left(\delta\frac{\partial w}{\partial t}\right)\right) + I_x(x)\omega_x\left(\delta\frac{\partial\theta}{\partial t} - \Omega_3\delta\frac{\partial w}{\partial x}\right) \\ &+ I_y(x)\omega_y\left(\delta\frac{\partial^2 w}{\partial t\partial x} + \Omega_1\theta\delta\frac{\partial w}{\partial x} + \Omega_1\frac{\partial w}{\partial x}\delta\theta + \Omega_3\delta\theta\right) \\ &+ I_z(x)\omega_z\left(-\theta\delta\frac{\partial^2 w}{\partial t\partial x} - \frac{\partial^2 w}{\partial t\partial x}\delta\theta + \Omega_1\delta\frac{\partial w}{\partial x}\right)\Bigg]\mathrm{d}x\,\mathrm{d}t.\end{aligned} \tag{A.3}$$

Integrating by parts, we get

$$\begin{aligned}\int_{t_1}^{t_2} \delta T_b\,\mathrm{d}t = &\int_{t_1}^{t_2}\int_0^L (-\rho(x)g\Omega_1\delta w)\,\mathrm{d}x\,\mathrm{d}t - \int_{t_1}^{t_2}\int_0^L \left(\rho(x)\frac{\partial h}{\partial t}\delta w\right)\mathrm{d}x\,\mathrm{d}t \\ &- \int_{t_1}^{t_2}\int_0^L \left(I_x(x)\frac{\partial\omega_x}{\partial t}\delta\theta\right)\mathrm{d}x\,\mathrm{d}t - \int_{t_1}^{t_2} I_x(x)\omega_x\Omega_3\delta w\big|_0^L\mathrm{d}t + \int_{t_1}^{t_2}\int_0^L \left(I_x(x)\Omega_3\frac{\partial\omega_x}{\partial x}\delta w\right)\mathrm{d}x\,\mathrm{d}t \\ &- \int_{t_1}^{t_2} \left(I_y(x)\frac{\partial\omega_y}{\partial t}\delta w\right)\Big|_0^L\mathrm{d}t + \int_{t_1}^{t_2}\int_0^L \left(I_y(x)\frac{\partial^2\omega_x}{\partial t\partial x}\delta w\right)\mathrm{d}x\,\mathrm{d}t + \int_{t_1}^{t_2} \left(I_y(x)\Omega_1\omega_y\theta\delta w\right)\big|_0^L\mathrm{d}t \\ &- \int_{t_1}^{t_2}\int_0^L \left(I_y(x)\Omega_1\frac{\partial}{\partial x}(\omega_y\theta)\delta w\right)\mathrm{d}x\,\mathrm{d}t + \int_{t_1}^{t_2}\int_0^L \left(I_y(x)\omega_y\Omega_1\frac{\partial w}{\partial x}\delta\theta\right)\mathrm{d}x\,\mathrm{d}t \\ &+ \int_{t_1}^{t_2}\int_0^L (I_y(x)\omega_y\Omega_3\delta\theta)\,\mathrm{d}x\,\mathrm{d}t + \int_{t_1}^{t_2}(I_z(x)\omega_z\Omega_1\delta w)|_0^L\,\mathrm{d}t - \int_{t_1}^{t_2}\int_0^L \left(I_z(x)\Omega_1\frac{\partial\omega_z}{\partial x}\delta w\right)\mathrm{d}x\,\mathrm{d}t.\end{aligned} \tag{A.4}$$

Simplifying and combining similar terms we get

$$\begin{aligned}\int_{t_1}^{t_2} \delta T_b\,\mathrm{d}t = \int_{t_1}^{t_2}\int_0^L \Bigg(&-\rho(x)g\Omega_1 - \rho_b\frac{\partial h}{\partial t} + I_x(x)\Omega_3\frac{\partial\omega_x}{\partial x} + I_y(x)\frac{\partial^2\omega_x}{\partial t\partial x} \\ &- I_y(x)\Omega_1\frac{\partial}{\partial x}(\omega_y\theta) - I_z(x)\Omega_1\frac{\partial\omega_z}{\partial x}\Bigg)\delta w\,\mathrm{d}x\,\mathrm{d}t - \int_{t_1}^{t_2}(I_x(x)\omega_x\Omega_3\delta w)|_0^L\,\mathrm{d}t\end{aligned}$$

$$+\int_{t_1}^{t_2}\int_0^L\left(-I_x(x)\frac{\partial\omega_x}{\partial t}+I_y(x)\omega_y\Omega_1\frac{\partial w}{\partial x}+I_y(x)\omega_y\Omega_3\right)\delta\theta\,\mathrm{d}x\,\mathrm{d}t$$
$$-\int_{t_1}^{t_2}\left(I_y(x)\frac{\partial\omega_y}{\partial t}\delta w\right)\Big|_0^L\mathrm{d}t+\int_{t_1}^{t_2}(I_y(x)\Omega_1\omega_y\theta\delta w)|_0^L\,\mathrm{d}t+\int_{t_1}^{t_2}(I_z(x)\omega_z\Omega_1\delta w)|_0^L\,\mathrm{d}t. \tag{A.5}$$

Total kinetic energy of the end mass is given as

$$T_M=\tfrac{1}{2}(M(f_M^2+g_M^2+h_M^2)+(I_{xM}\omega_x^2+I_{yM}\omega_y^2+I_{zM}\omega_z^2)). \tag{A.6}$$

Taking the variation of the above expression yields

$$\int_{t_1}^{t_2}\delta T_M\,\mathrm{d}t=\int_{t_1}^{t_2}(M(f_M\delta f_M+g_M\delta g_M+h_M\delta h_M)+I_{xM}\omega_x\delta\omega_x+I_{yM}\omega_y\delta\omega_y+I_{zM}\omega_z\delta\omega_z)\,\mathrm{d}t. \tag{A.7}$$

Substituting values of f_M, g_M, h_M, ω_x, ω_y and ω_z from Eqs. (11) and (21), we can simplify the above expression as follows:

$$\begin{aligned}\int_{t_1}^{t_2}\delta T_M\,\mathrm{d}t=\int_{t_1}^{t_2}\Bigg(&M\left(\left(-g_M\Omega_1-\frac{\partial h_M}{\partial t}\right)\delta w_L-\left(\Omega_1\frac{l_M}{2}+\frac{l_M}{2}\frac{\partial h_M}{\partial t}\right)\delta\frac{\partial w}{\partial x}\Big|_{x=L}\right)\\&-I_{xM}\omega_x\Omega_3\delta\frac{\partial w}{\partial x}\Big|_{x=L}-I_{xM}\frac{\partial(\omega_x)}{\partial t}\delta\theta_L-I_{yM}\frac{\partial(\omega_y)}{\partial t}\frac{\partial w}{\partial x}\Big|_{x=L}\\&+I_{yM}\omega_y\Omega_1\theta\frac{\partial w}{\partial x}\Big|_{x=L}+I_{yM}\omega_y\Omega_1\frac{\partial w}{\partial x}\delta\theta_L+I_{yM}\omega_y\Omega_3\delta\theta_L\\&+I_{zM}\omega_z\Omega_1\delta\frac{\partial w}{\partial x}\Big|_{x=L}\Bigg)\mathrm{d}t.\end{aligned} \tag{A.8}$$

Potential energy:

$$\begin{aligned}\int_{t_1}^{t_2}\delta V\,\mathrm{d}t&=\int_{t_1}^{t_2}\int_0^L\left[EI_y(x)\left(\frac{\partial^2 w}{\partial x^2}\right)\delta\left(\frac{\partial^2 w}{\partial x^2}\right)+GJ(x)\left(\frac{\partial\theta}{\partial x}\right)\delta\left(\frac{\partial\theta}{\partial x}\right)\right]\mathrm{d}x\,\mathrm{d}t\\&=\int_{t_1}^{t_2}EI_y(x)\left(\frac{\partial^2 w}{\partial x^2}\right)\delta\left(\frac{\partial w}{\partial x}\right)\Big|_0^L\mathrm{d}t-\int_{t_1}^{t_2}EI_y(x)\left(\frac{\partial^3 w}{\partial x^3}\right)\delta w\Big|_0^L\mathrm{d}t\\&\quad+\int_{t_1}^{t_2}\int_0^L\left(EI_y(x)\left(\frac{\partial^4 w}{\partial x^4}\right)\delta w\right)\mathrm{d}x\,\mathrm{d}t+\int_{t_1}^{t_2}GJ(x)\left(\frac{\partial\theta}{\partial x}\right)\delta\theta\Big|_0^L\mathrm{d}t\\&\quad-\int_{t_1}^{t_2}\int_0^L\left(GJ(x)\left(\frac{\partial^2\theta}{\partial x^2}\right)\delta\theta\right)\mathrm{d}x\,\mathrm{d}t.\end{aligned} \tag{A.9}$$

Simplifying and combining similar terms we get

$$\begin{aligned}\int_{t_1}^{t_2}\delta V\,\mathrm{d}t=&\int_{t_1}^{t_2}\int_0^L\left(EI_y(x)\left(\frac{\partial^4 w}{\partial x^4}\right)\right)\delta w\,\mathrm{d}x\,\mathrm{d}t-\int_{t_1}^{t_2}\int_0^L\left(GJ(x)\left(\frac{\partial^2\theta}{\partial x^2}\right)\right)\delta\theta\,\mathrm{d}x\,\mathrm{d}t\\&+\int_{t_1}^{t_2}EI_y(x)\left(\frac{\partial^2 w}{\partial x^2}\right)\delta\left(\frac{\partial w}{\partial x}\right)\Big|_0^L\mathrm{d}t-\int_{t_1}^{t_2}EI_y(x)\left(\frac{\partial^3 w}{\partial x^3}\right)\delta w\Big|_0^L\mathrm{d}t+\int_{t_1}^{t_2}GJ(x)\left(\frac{\partial\theta}{\partial x}\right)\delta\theta\Big|_0^L\mathrm{d}t.\end{aligned} \tag{A.10}$$

Virtual work is represented as

$$\delta W_{\mathrm{nc}}=\frac{1}{2}\int_0^L\frac{\partial^2 M_P}{\partial x^2}\delta w\,\mathrm{d}x+C_B\int_0^L\frac{\partial w}{\partial t}\delta w\,\mathrm{d}x+C_T\int_0^L\frac{\partial\theta}{\partial t}\delta\theta\,\mathrm{d}x, \tag{A.11}$$

where [18]

$$M_p=-\tfrac{1}{2}bE_pd_{31}(t_b+t_p)V_p(t)S(x)=M_{p0}V_p(t)S(x), \tag{A.12}$$

$$S(x)=H(x-l_1)-H(x-l_2).$$

Using Eqs. (A.1)–(A.12) and taking into account the fact that δw, $\delta\theta$, δw_L and $(\partial/\partial x)\delta w_L$ could have any arbitrary values, the coefficients of these terms in Hamilton's equation must vanish. Hence, after substituting values of g,h,ω_x, ω_y, ω_z and ignoring rotary inertia for the beam, the equations of motion and boundary conditions can be obtained as given in Eqs. (27)–(32).

References

[1] E. Kanso, A.J. Szeri, A. Pisano, Cross-coupling errors of micromachined gyroscopes, *Journal of Microelectromechanical Systems* 13 (2) (2004) 323–331.

[2] N. Yazdi, F. Ayazi, K. Najafi, Micromachined inertial sensors, *Proceedings of the IEEE* 86 (8) (1996) 1640–1659.

[3] M. Esmaeili, M. Durali, N. Jalili, Dynamic modeling and performance evaluation of a vibrating microgyroscope under general support motion, *Journal of Sound and Vibration* 301 (1) (2007) 146–164.

[4] S. Timoshenko, D.H. Young, *Vibration Problems in Engineering*, Van Nostrand, New York, 1955.

[5] E. Dokumaci, An exact solution for coupled bending and torsion vibrations of uniform beams having single cross-sectional symmetry, *Journal of Sound and Vibration* 119 (1987) 443–449.

[6] A.N. Bercin, M. Tanaka, Coupled flexural–torsional vibrations of Timoshenko beams, *Journal of Sound and Vibration* 207 (1) (1997) 47–59.

[7] J.R. Banerjee, Explicit frequency equation and mode shapes of a cantilever beam coupled in bending and torsion, *Journal of Sound and Vibration* 224 (2) (1999) 267–281.

[8] R.P. Goel, Vibrations of a beam carrying a concentrated mass, *Journal of Applied Mechanics* 40 (1974) 421–422.

[9] P.A.A. Laura, J.L. Pombo, E.A. Susemihl, A note on the vibrations of a clamped-free beam with a mass at the free end, *Journal of Sound and Vibration* 37 (1974) 161–168.

[10] R. Bhat, H. Wagner, Natural frequencies of a uniform cantilever with a tip mass slender in the axial direction, *Journal of Sound and Vibration* 45 (1976) 304–307.

[11] C.L. Kirk, S.M. Weidemann, Natural frequencies and mode shapes of a free–free beam with large end masses, *Journal of Sound and Vibration* 254 (5) (2002) 939–949.

[12] D.C.D. Oguamanam, Free vibration of beams with finite mass rigid tip load and flexural–torsional coupling, *International Journal of Mechanical Sciences* 45 (2003) 963–979.

[13] H. Gokdag, O. Kopmaz, Coupled bending and torsional vibrations of a beam with tip and in-span attachments, *Journal of Sound and Vibration* 287 (2005) 591–610.

[14] M. Esmaeili, M. Durali, N. Jalili, Modeling and vibration analysis of vibrating beam microgyroscopes under longitudinal rotation of the support, *Proceedings of 2005 ASME International Mechanical Engineering Conference & Exposition*, Orlando, FL, November 5–11, 2005.

[15] M. Esmaeili, M. Durali, N. Jalili, Closed form solutions of frequency equations for a cantilever flexible beam under general base excitation, *Proceedings of ASME International Design Engineering Technical Conferences and Information in Engineering Conferences 20th Biennial Conference on Mechanical Vibration and Noise*, Long beach, CA, September 24–28, 2005.

[16] M. Esmaeili, M. Durali, N. Jalili, Ring microgyroscope modeling and performance evaluation, *Journal of Vibration and Control* 12 (5) (2006) 537–553.

[17] P. Malatkar, Nonlinear Vibrations of Cantilever Beams and Plates, PhD Dissertation, Virginia Polytechnic Institute and State University, 2003.

[18] M. Dadfarnia, N. Jalili, B. Xian, D. Dawson, A Lyapunov-based piezoelectric controller of flexible cartesian robot manipulators, *ASME Journal of Dynamic Systems, Measurement and Control* 126 (2) (2004) 347–358.

[19] M. Dadfarnia, N. Jalili, Z. Liu, D. Dawson, An observer-based piezoelectric control of flexible cartesian robot arms: theory and experiment, *Control Engineering Practice* 12 (2004) 1041–1053.

[20] S. Rajendran, K.M. Liew, Design and simulation of an angular-rate vibratory microgyroscope, *Sensors and Actuators: A. Physica* 116 (2) (2004) 241–256.

[21] W. Geiger, B. Folkmer, U. Sobe, H. Sandmaier, W. Lang, New designs of micromachined vibrating rate gyroscopes with decoupled oscillation modes, *Sensors and Actuators: A. Physical* 66 (1998) 118–124.

[22] V. Bhadbhade, N. Jalili, Coupled flexural–torsional vibrations of a Piezoelectrically-actuated vibrating beam gyroscope, *Proceedings of 2006 ASME International Mechanical Engineering Conference & Exposition*, Chicago, IL, November 5–10, 2006.